Rigid Motion Compensation in Interventional C-arm CT Using Consistency Measure on Projection Data

Robert Frysch and Georg Rose

Institute for Medical Engineering, University of Magdeburg, Germany
robert.frysch@ovgu.de

Abstract. Interventional C-arm CT has the potential to visualize brain hemorrhages in the operating suite and save valuable time for stroke patients. Due to the critical constitution of the patients, C-arm CT images are frequently affected by patient motion artifacts, which often makes the reliable diagnosis of hemorrhages impossible. In this work, we propose a geometric optimization algorithm to compensate for these artifacts and present first results. The algorithm is based on a projection data consistency measure, which avoids computationally expensive forward- and backprojection steps in the optimization process. The ability to estimate movements with this measure is investigated for different rigid degrees of freedom. It was shown that out-of-plane parameters, i. e. geometrical deviations perpendicular to the plane of rotation, can be estimated with high precision. Movement artifacts in reconstructions are consistently reduced throughout all analyzed clinical datasets. With its low computational cost and high robustness, the proposed algorithm is well-suited for integration into clinical software prototypes for further evaluation.

1 Introduction

The soft tissue contrast resolution of C-arm based computed tomography (CT) has been continuously improved over the past decade. Recent publications already demonstrate good visibility of brain hemorrhages [11]. However, the application of the interventional C-arm for the acute stroke assessment, providing the ability for stroke diagnosis in the operating room, requires a reliable detection of even very small bleedings also in the vicinity of bones. In order to meet these requirements, one has to overcome image quality disturbances caused by beam hardening, poor scatter compensation and particularly motion of the patients during the long acquisition times.

We are targeting a motion compensation method for C-arm CT which neither depends on additional measurements nor requires assumptions or information about the object's shape. Various methods can be found in the literature discussing geometric calibration and motion compensation, which are closely related. Certain approaches are based on volumetric reconstructions in the optimization processes. Either the objective function determines the similarity of

N. Navab et al. (Eds.): MICCAI 2015, Part I, LNCS 9349, pp. 298–306, 2015.
DOI: 10.1007/978-3-319-24553-9_37

simulated and measured projections (2D-3D registration) [8] or operates in the volume domain quantifying geometric misadjustment with an artifact measure ("symptomatical approach") [5]. Other approaches, like the proposed, operate only on the redundancies in the projection images. Therefore, computationally intensive reconstruction within the optimization procedure becomes obsolete, allowing for very short overall processing time. Epipolar geometry is typically used to identify redundancies [12,7]. Debbeler et al. [3] introduced a novel online geometric calibration approach for industrial CT using a global optimization of several geometric parameters of the CT alignment (e. g. detector shift). This approach was extended in Maass et al. [6] to a local adaption of the geometry of each projection image. It benefits from a robust consistency measure, which exploits redundancies in the complete acquired projection data based on Grangeat's fundamental relation for cone-beam CT [4]. A reformulation of this consistency measure for the context of epipolar geometry is provided by Aichert et al. [2,1]. Therein, a simulation study was performed for the compensation of artificial geometry shifts in small sets of cone-beam projections. In this work, we adapt this strategy to real C-arm short scans, i. e. a cone-beam geometry with semicircle trajectory. We present first reconstruction results of rigid motion compensation for real patient data based on the consistency measure.

At first, we investigated the ability of this approach to estimate the motion parameters for several degrees of freedom. Based on these insights, we applied a customized geometry optimization procedure to projections from five clinical datasets. This geometric adaptation was followed by a standard reconstruction (FDK). Reconstructed images without motion compensation were used for comparison.

2 Methods

2.1 Objective Function

One can define a consistency measure based on redundancies occurring in CT projection datasets. For this, we consider a plane $\{\mathbf{n}, l\}$: $\{\mathbf{x} \in \mathbb{R}^3 \,|\, \mathbf{n} \cdot \mathbf{x} = l\}$ in the patient's world coordinate system with the normal unit vector $\mathbf{n}$ and the distance l to the origin. The projection's redundancies manifest in Grangeat's fundamental relation which connects the 3D Radon transform[1] $r(\mathbf{n}, l)$ with an intermediate function $S_i(\mathbf{n})$ (cf. Defrise et al. [4]):

$$S_i(\mathbf{n}) := -\int_{S^2} \mathsf{d}\mathbf{m}\, \delta'(\mathbf{m} \cdot \mathbf{n}) g_i(\mathbf{m}) = \frac{\partial}{\partial l}\, r(\mathbf{n}, l)|_{l=\mathbf{C}_i \cdot \mathbf{n}} \,. \tag{1}$$

$\mathbf{C}_i$ denotes the vector to the point of the i'th x-ray source position lying on the plane. The intermediate function $S_i(\mathbf{n})$ is a transformation of the cone-beam projections $g_i(\mathbf{m})$ (also called X-ray transform; alternative representation of the 2D projection images $g_i(x, y)$), where $\mathbf{m}$ is the direction of a ray starting from $\mathbf{C}_i$. The integration is over the unit 2-sphere and $\delta'(x)$ is the derivative of the

[1] 3D radon transform: integrals over 2D planes of a three-dimensional scalar field.

Dirac delta distribution. Thus, there are only contributions from $g_i(\mathbf{m})$, when $\mathbf{m}$ is perpendicular to $\mathbf{n}$. In other words the integration is reduced to an 1D manifold considering only x-rays which lie within the plane $\{\mathbf{n}, l = \mathbf{C}_i \cdot \mathbf{n}\}$, i. e. add up projection values located at the line of intersection between this plane and the detector plane. As a consequence, it is appropriate to identify the plane $\{\mathbf{n}, l\}$ with the intersection line in the i'th detector coordinate system using conventional 2D Radon parametrization $\{\vartheta, s\}$ (ϑ denotes the angle of the line's normal and s the distance to origin). The coordinate transformation to Radon parameters of the i'th local system $\{\mathbf{n}, l\} \rightarrow \{\vartheta, s\}_i$ in the integral (1) can also be found in Defrise et al. [4]. Its rewritten result is:

$$S_i(\vartheta, s) = \frac{s^2 + D^2}{D^2} \cdot \frac{\partial}{\partial s} \Re\left[\tilde{g}_i\right](\vartheta, s), \text{ with } \tilde{g}_i(x, y) = \frac{D}{\sqrt{x^2 + y^2 + D^2}} \cdot g_i(x, y)\,. \tag{2}$$

D is the source-detector distance and $\Re\left[\,.\,\right](\vartheta, s)$ the 2D Radon transform (parallel beam) which has to be applied to cosine weighted projections $\tilde{g}_i(x, y)$.

Assuming a static object, the expression at the right-hand side of Grangeat's equation (1) depends only on the plane $\{\mathbf{n}, l\}$. By selecting another projection g_j with source position $\mathbf{C}_j$ which also fulfills $l = \mathbf{C}_j \cdot \mathbf{n}$, i. e. it is located in the same plane, one can conclude that the intermediate function values $S_i(\mathbf{n}) = S_i(\vartheta_i, s_i)$ and $S_j(\mathbf{n}) = S_j(\vartheta_j, s_j)$ are equal. Now, we can fix the source positions and consider N different planes with normal vectors $\mathbf{n}^n$ for which $\mathbf{C}_i \cdot \mathbf{n}^n = \mathbf{C}_j \cdot \mathbf{n}^n$ holds true. For each of these planes redundant pairs $S_i(\vartheta_i^n, s_i^n) \overset{!}{=} S_j(\vartheta_j^n, s_j^n)$ from two projections can be found.

We define the following error matrix (norm type) describing the consistency of each combination of two projection images:

$$\varepsilon_{ij} := \frac{1}{N} \sum_{n=1}^{N} \left| S_i(\vartheta_i^n, s_i^n) - S_j(\vartheta_j^n, s_j^n) \right|^p, \quad N \overset{\text{gen.}}{=} N_{ij}\,.$$

The parameter p controls properties of this metric like smoothness, detectability of inconsistencies or consideration of outliers and has to be chosen empirically. We figured out a reliable value of $p = 0.3$ in simulations and used it throughout all experiments. In general, the number of available mutual planes N containing $\mathbf{C}_i$ and $\mathbf{C}_j$ depends on i and j. This is due to divergent geometric situations of combinations of two C-arm positions and the finiteness of the detector (more detailed in section 2.3). A summation of the error function ε_{ij} enables us to quantify the consistency of a set of projections with indices $\mathbf{I} = \{i_1, \ldots, i_I\}$ with respect to all the other J existing projections:

$$E_{\mathbf{I}} := \sum_{i \in \mathbf{I}} \sum_{j \notin \mathbf{I}} \varepsilon_{ij}\,.$$

Thus, we obtain an objective function for a given set of I projection images containing $\overline{N} \times I \times J$ redundant pairs of values (with $\overline{N}$ as a corresponding average of N_{ij}). In the special case of considering only one projection angle i,

we obtain $E_i = \sum_{j \neq i} \varepsilon_{ij}$. The high quantity of redundant pairs provides a good basis for an optimization which is robust in terms of noise.

2.2 Optimization Procedure

We define a world coordinate system which is orientated in such a way that the z-axis is parallel to the C-arm's rotational axis. Our optimization approach for a rigid geometric modification is based on the following parameter set

$$\triangle \mathbf{p} := \begin{bmatrix} \boldsymbol{\alpha} \\ \boldsymbol{\tau} \end{bmatrix}, \text{with } \boldsymbol{\tau} = \begin{bmatrix} \tau_x \\ \tau_y \\ \tau_z \end{bmatrix}, \ \boldsymbol{\alpha} = \begin{bmatrix} \alpha_x \\ \alpha_y \\ \alpha_z \end{bmatrix},$$

thus including a shift of the world coordinate system by a vector $\boldsymbol{\tau}$ as well as a rotation w.r.t. the axis $\boldsymbol{\alpha}$ by an angle $\|\boldsymbol{\alpha}\|$. It defines a useful dependency of the objective function $E_{\mathbf{I}} = E_{\mathbf{I}}(\triangle \mathbf{p})$ without ambiguous points in the 6D optimization space. Moreover, we can separate these geometric changes into two distinctive groups:

$$\text{out-of-plane parameters: } \triangle \mathbf{p}_{\mathsf{OP}} = \begin{bmatrix} \alpha_x \\ \alpha_y \\ t_z \end{bmatrix}, \text{ in-plane parameters: } \triangle \mathbf{p}_{\mathsf{IP}} = \begin{bmatrix} \alpha_z \\ t_x \\ t_y \end{bmatrix}.$$

Due to the semicircle geometry of the short scan, most projections do not have opposing views. Therefore, planes including X-ray sources of such projections and hitting the (limited) detector can only be slightly tilted from the plane of rotation. It was expected that the intermediate function values of those would not be susceptible to modifications of in-plane (IP) parameters, because the according 3D Radon transform value is not affected by translations/rotations within those planes (or planes parallel to them). On the contrary, geometric variations stepping out of the plane of rotation should significantly change the consistency error ε_{ij}.

This expectation was confirmed by simulations with a 3D Shepp-Logan phantom. In figure 1, only one of the six parameters $\triangle \mathbf{p}$ is changed from a perfect semicircle trajectory for each angle (row) and its consistency error ε_{ij} is determined by the unaltered other angles (columns). One can observe significant increases in the error function throughout all projections when changing one of the out-of-plane (OP) parameters $\triangle \mathbf{p}_{\mathsf{OP}}$. In contrast, when modifying IP parameters $\triangle \mathbf{p}_{\mathsf{IP}}$, the consistency measure is only sensible for the first and last projections, which represent opposite views and offer the most redundancy. To be more precise, this includes all projections containing identical rays (angular range equals to two times of the opening angle of the fan). In the following these projections will be referred to as the "fan angle sector".

Considering these findings, a separate optimization of the three OP parameters was performed for each single projection. If required, optimization can be extended to the full 6D $\triangle \mathbf{p}$ inside the fan angle sector as well as the inter-fan angle sector, if we increase the angle block length I, e. g. $I = 2$ (for fan angle

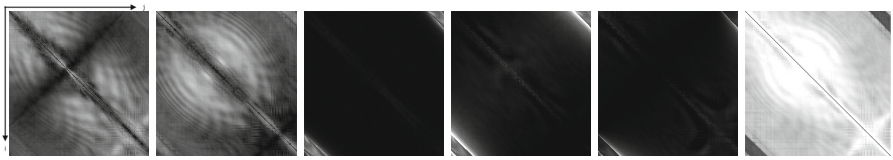

(a) α_x (b) α_y (c) α_z (d) τ_x (e) τ_y (f) τ_z

Fig. 1. Consistency measure ε_{ij} of each single rigid degree of freedom. For each defined geometry parameter, the increase of the error matrix ε_{ij} is depicted for misadjustments between two projections at row i and column j of 0.5 ° or 0.5 mm, respectively. The same grey scale window is used for each matrix. The largest increase of the error can be observed for the OP parameter in (a), (b) and (f).

sector) and $I = 15$ (for inter-fan angle sector). Optimizing a larger block of $\mathbf{I}$ results in a higher number of redundant pairs in the objective function leading to more support. However, a further consequence of the increased block size, the estimation of the geometry of projections with rapid patient motion is hampered.

2.3 Implementation

The intermediate function was computed on the CPU before the actual optimization routine. This function was then sampled and stored for the optimization process in the GPU's video RAM:

1. cosine weighting of $g_i(x, y)$
2. Radon transformation based on the model of Siddon [10] with a sampling rate of $\Delta s = 1$ Pixel and $\Delta\vartheta = 0.5\,^\circ$
3. numerical differentiation with respect to s (centered derivative filter $[-1, 0, 1]$) and weighting according to (2)

The weightings in steps 1. and 2. could be computed as pre-processing steps since the intrinsic parameter of the C-arm system were fixed within the optimization routine. The sampling rates Δs und $\Delta\vartheta$ of the Radon transformation were determined empirically by selecting the configuration with the lowest numerical error in the simulations.

The essential part of the optimization represents the search for the redundant Radon pairs $(\vartheta_i, s_i) \leftrightarrow (\vartheta_j, s_j)$ of two projections required to determine the ε_{ij}. For that, we used the constraint that two source positions $\mathbf{C}_i$ and $\mathbf{C}_j$ are on the same plane. An intuitive way of gathering the related set of planes is to rotate an initial plane around a line connecting the two sources by an angle ϕ. Using this strategy, we were able to estimate several redundant pairs of intermediate function values by a fast linear interpolation on video the GPU's RAM. Thereby, only those planes with intersection lines $\{\vartheta, s\}_{i/j}$ located inside both detector areas were considered. The smallest reasonable change $\Delta\phi$ of the plane rotation is given by the sampling of the Radon transformation. It was estimated through geometric consideration (not shown here). Using the above

parameters and the geometry of a Siemens Artis Q C-arm with source-detector distance $D = 1.2\,\mathrm{m}$, detector resolution of $0.308 \times 0.308\,\mathrm{mm}$ and 1240×960 pixels, we estimated a lower bound of $\Delta\phi \approx 0.015\,°$, resulting in a maximum number of redundant pairs $N_{\mathsf{max}} = \frac{180\,°}{\Delta\phi} \approx 12,000$. As already mentioned in section 2.1, this amount is not attainable for all projection combinations when using equidistant rotational steps. Especially, the overall amount for each angle is not equally distributed, due to limited angle of rotation (approx. 200 °) in short scans (in connection with limited detector size). The number of usable planes (associated with available redundant values) is shown in figure 2.

The computation of the objective function $E_{\mathbf{I}}$ was performed for each ε_{ij} in parallel on GPU using OpenCL programming language. For minimization of the objective function, we used a nonlinear optimization algorithm from the open-source library NLopt[2] which is based on T. Rowan's "Subplex" [9] implementation.

In summary, the main methodical differences to the work of Maass et al. [6] are: nonlinear optimizer instead of grid search, multidimensional optimizing of the world coordinate system instead of single intrinsic CT geometry parameters (motion instead of calibration), $p = 0.3$ instead of $p = 2$ (smoothing the objective function), $N_{\mathsf{max}} = 12,000$ instead of $N_{\mathsf{max}} = 768$.
With these adaptions, we tried to overcome the inferior preconditions of the C-arm in terms of data quality (e. g. partial overexposure) and short-scan geometry.

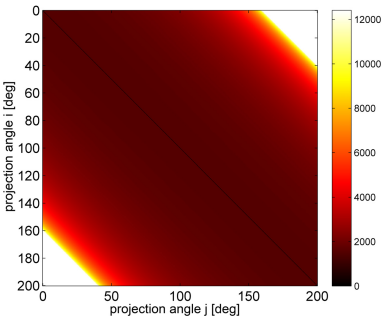

Fig. 2. Number of usable redundant Radon planes for each X-ray image pair of a short scan (0 ° . . . 200 °). Most of the planes are concentrated at the fan angle sector containing opposite views.

3 Results

A Siemens Artis Q system has been used to acquire the clinical data using a 20 sec protocol with 496 projection images. Figure 3 depicts the effect of the optimization on the error matrix ε_{ij}. In this example, the acquisition of a patient head with distinct movements was used. One can notice an increase of the consistency error ε_{ij} as well the totalized $E_i = \sum_j \varepsilon_{ij}$ for the misadjusted projections. The peaks in figure 3b are correlated with the amount of geometric changes after the optimization. The optimization was performed sequentially through all images, but was applied for all three OP parameter at once. Figure 4 depicts the improvement of the reconstruction (via FDK) in four datasets after the 3D OP optimization which was already sufficient in most cases. However, Figure 5

[2] Steven G. Johnson, The NLopt nonlinear-optimization package.

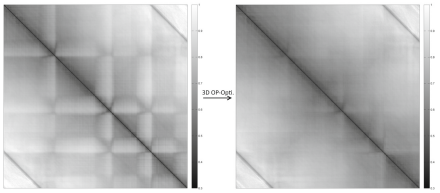

(a) Error matrix ε_{ij} before (left) and after (right) the optimization. Reconstructions are shown in the upper right in figure 4.

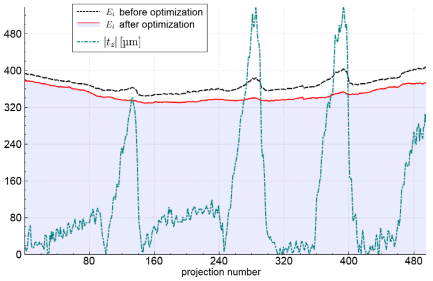

(b) Totalized Error E_i before and after the 3D OP optimization and the absolute value of the resulting OP parameter t_z.

Fig. 3. Impact of a sequential 3D OP parameter optimization on the consistency metric ε_{ij}, its summation E_i over columns and the translations $\{t_z\}_i$ in $\triangle \mathbf{p}_{\mathsf{OP}}$

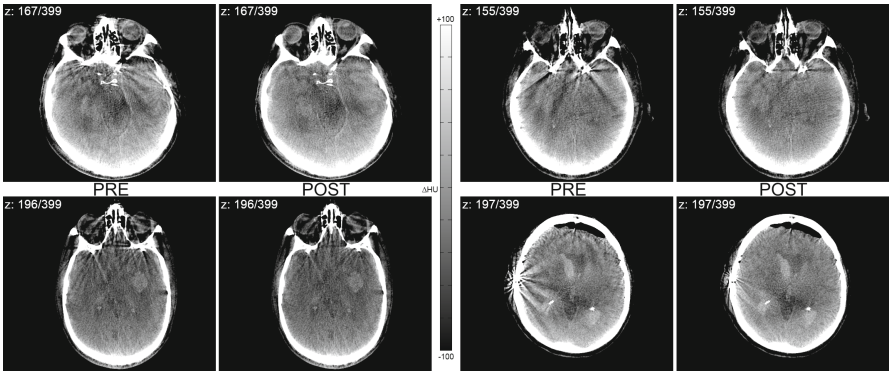

Fig. 4. Reconstructions of four clinical datasets before and after a sequential 3D OP motion compensation (very robust). Computation time per patient is about 30 sec using a standard gaming videocard AMD Radeon R9 280.

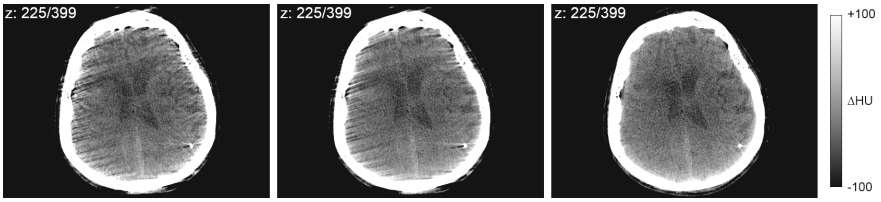

Fig. 5. Reconstruction with uncorrected geometry (left), after a sequential 3D OP motion compensation (center) and subsequent full 6D optimization (OP+IP).

presents a case where a 6D optimization of the whole parameter vector $\triangle \mathbf{p}$ provides further improvement of image quality. Note that the 6D optimization is unstable in general and does not improve image quality in every case. This will be subject of future work.

4 Conclusions

In this work we show the possibility to compensate rigid patient motion in the out-of-plane parameters, which can be performed in a robust manner. These parameters can be separated from the other geometric directions and optimized in a 3D nonlinear minimization procedure. This leads to a robust motion compensation of the reconstructed images at a relatively low computational cost. In most cases, it was sufficient to neglect the in-plane parameters which are, in general, difficult to optimize. However, assumably, they have minor influence on the image quality. In one case, it was beneficial to consider all six degrees of freedom which was realized by optimizing a larger block of projections at once. Limitations may occur, if there are further artefacts within the projections due to truncation, detector overexposure or beam hardening. A refinement of the optimization strategy, e. g. the detection of motion based on pattern recognition in the error matrix ε_{ij}, can reduce the computational cost.

Acknowledgment. The work of this paper is partly funded by the German BMBF within the Forschungscampus *STIMULATE* (13GW0095A).

References

1. Aichert, A., Berger, M., Wang, J., Maass, N., Doerfler, A., Hornegger, J., Maier, A.: Epipolar consistency in transmission imaging. IEEE TMI (2015). Epub ahead of print, doi:10.1109/TMI.2015.2426417
2. Aichert, A., Maass, N., Deuerling-Zheng, Y., Berger, M., Manhart, M., Hornegger, J., Maier, A., Doerfler, A.: Redundancies in x-ray images due to the epipolar geometry for transmission imaging. In: Third CT Meeting, pp. 333–337 (2014)
3. Debbeler, C., Maass, N., Elter, M., Dennerlein, F., Buzug, T.M.: A new CT rawdata redundancy measure applied to automated misalignment correction. In: 12th Fully 3D, pp. 264–267 (2013)
4. Defrise, M., Clack, R.: A cone-beam reconstruction algorithm using shift-variant filtering and cone-beam backprojection. IEEE TMI 13(1), 186–195 (1994)
5. Kyriakou, Y., Lapp, R.M., Hillebrand, L., Ertel, D., Kalender, W.A.: Image-based online correction of misalignment artifacts in cone-beam CT. In: SPIE, vol. 7258, pp. 72581V–72581V–10 (2009)
6. Maass, N., Dennerlein, F., Aichert, A., Maier, A.: Geometrical jitter correction in computed tomography. In: Third CT Meeting, pp. 338–342 (2014)
7. Meng, Y., Gong, H., Yang, X.: Online geometric calibration of cone-beam computed tomography for arbitrary imaging objects. IEEE TMI 32(2), 278–288 (2013)
8. Muders, J., Hesser, J.: Stable and robust geometric self-calibration for cone-beam CT using mutual information. IEEE TNS 61(1), 202–217 (2014)
9. Rowan, T.: Functional Stability Analysis of Numerical Algorithms. Ph.d. thesis, University of Texas at Austin, Department of Computer Sciences (1990)

10. Siddon, R.L.: Fast calculation of the exact radiological path for a three-dimensional CT array. Medical Physics 12, 252–255 (1985)
11. Söderman, M., Babic, D., Holmin, S., Andersson, T.: Brain imaging with a flat detector C-arm. Neuroradiology 50, 863–868 (2008)
12. Wein, W., Ladikos, A.: Detecting patient motion in projection space for cone-beam computed tomography. In: Fichtinger, G., Martel, A., Peters, T. (eds.) MICCAI 2011, Part I. LNCS, vol. 6891, pp. 516–523. Springer, Heidelberg (2011)